The central role of the Atlantic meridional overturning circulation in the Bjerknes compensation

Yoania Povea-Pérez, Éric Guilyardi, Alexey Fedorov, Brady Ferster

The central role of the Atlantic meridional overturning circulation in the Bjerknes compensation

The central role of the Atlantic meridional overturning circulation in the Bjerknes compensation

Yoania Povea Pérez[1*], Éric Guilyardi[1,2], Alexey Fedorov[1,3], Brady Ferster[1]

[1]*LOCEAN-IPSL, (Sorbonne Université, CNRS, IRD, MNHN), Paris, France.*

[2]*NCAS-Climate, University of Reading, Reading, UK.*

[3]*Department of Earth and Planetary Sciences, Yale University, New Haven, CT, USA.*

*Corresponding author e-mail:
yoania.povea-perez@locean.ipsl.fr

Abstract

Poleward heat (energy) transport plays a major role in shaping the Earth's climate. Its oceanic and atmospheric components carry heat from low to high latitudes thus reducing the equator-to-pole temperature contrast. In quasi-equilibrium climate states, changes in the top-of-the-atmosphere (TOA) energy fluxes and ocean heat content remain small. In such conditions, anomalies in oceanic and atmospheric heat transport must have the same magnitude but opposite signs (Bjerknes, 1964). This phenomenon is known as the Bjerknes compensation (BJC). The BJC hypothesis is of high importance in climate, since it imposes a strong constraint on climate variability at sufficiently long timescales (on sub-decadal and shorter timescales TOA flux variations may become comparable to other heating terms, interfering with BJC). However, to which extent BJC operates in the climate system and the key mechanisms of the compensation remain poorly understood. Here we analyze BJC in the IPSL-CM6A-LR climate model, focusing on its timescale dependence, its links to the Atlantic Meridional Overturning Circulation (AMOC), and the connection to Intertropical Convergence Zone (ITCZ) shifts. We show that BJC occurs in the model at both multi-decadal and centennial timescales, but is stronger on centennial timescales than decadal. In both cases BJC is initiated by variations in ocean heat transport induced by AMOC variability that are partially or fully compensated by atmospheric heat transport. For decadal timescales, we find two regions of a strong BJC associated with the storm track region and the marginal ice zone in the Northern Hemisphere. Finally, on centennial timescales we observe a Bjerknes-like interbasin compensation between the Atlantic and Indo-Pacific heat transports, which is also related to strong centennial AMOC fluctuations and involves Southern Ocean zonal heat transport.

Keywords: poleward heat transport, Bjerknes compensation, Atlantic Meridional Overturning Circulation, AMOC, climate variability.

1. Introduction

The Earth's climate is fundamentally controlled by solar radiation. Likewise, meridional heat transport from low to high latitudes, resulting from the heating contrast between the equator and polar regions and partitioned between oceanic (OHT) and atmospheric (AHT) heat transports, is essential for shaping the climate and maintaining the Earth energy balance. In equilibrium, the planetary heat transport is linked to the net heat flux at the top of the atmosphere (TOA). On decadal and longer timescales OHT anomalies are primarily driven by the Atlantic Meridional Overturning Circulation (AMOC) (Oldenburg et al., 2021; Shaffrey & Sutton, 2006) and the wind-driven subtropical cells (Ferrari & Ferreira, 2011; Klinger & Marotzke, 2000), while AHT anomalies depend on atmospheric meridional overturning circulation (Held, 2001) and mid-latitudes baroclinic eddies (Barry et al., 2002).

In a statistical equilibrium, changes in TOA net heat flux and in heat storage by the ocean are an order of magnitude smaller than anomalous convergence of oceanic or atmospheric heat transports. In such conditions, changes in OHT are accompanied by corresponding AHT anomalies of approximately the same magnitude and opposite sign, and vice versa. This conjecture, initially proposed by (Bjerknes, 1964) is referred to as the Bjerknes Compensation (BJC). At sub-decadal timescales changes in OHT are typically offset by changes in oceanic heat storage, given the large heat capacity of the ocean. Consequently, BJC should operate on decadal and longer timescales. As long measurements in the ocean are scarce, BJC remains an

hypothesis that is challenging to prove through direct observations (Yang et al., 2013). Therefore, using climate models can provide valuable insights into the ocean-atmosphere coupling processes. Furthermore, anthropogenic activity has altered the atmospheric composition and radiative budget of the planet (Masson-Delmotte et al., 2021), inducing large-scale increases in the world's oceans heat content (Barnett et al., 2001). Thus, understanding energy compensation mechanisms and their potential role in climate change remains an important task.

The BJC idea and its mechanisms have received increased attention in recent decades. Several studies (Dai et al., 2017; Z. Liu et al., 2016; Yang et al., 2015, 2017) have shown that BJC is closely linked to local climate feedbacks (e.g. affecting the relationship between the net heat flux at the TOA and temperature at the surface), so that negative local feedbacks and ocean heat storage can lead to AHT anomalies undercompensating OHT changes and vice versa.

Because of limited observations and long-timescales needed, climate models of various complexity remain the main tool to study BJC. These models range from Energy Balance Models (Z. Liu et al., 2016) and conceptual box models (Yang et al., 2015, 2016) to general circulation coupled climate models (GCMs) (Jungclaus & Koenigk, 2010; Outten et al., 2018; Outten & Esau, 2017; van der Linden et al., 2019). Coupled GCMs have been used to analyze ocean-atmosphere energy compensation in natural climate variability (Jungclaus & Koenigk, 2010; Lucarini & Ragone, 2011; Outten & Esau, 2017) and in forced realistic and idealized climate scenarios (He et al., 2019; Lucarini & Ragone, 2011; Rose & Ferreira, 2012; van der

Linden et al., 2019; Yang et al., 2015, 2015). These studies have demonstrated that BJC occurs in these models and is a function of latitude and timescales considered.

Despite efforts to elucidate BJC underlying mechanisms, several questions remain unanswered. For instance, a recent study (Shaffrey & Sutton, 2006) proposed as a possible interpretation for BJC dependence on timescales that the atmosphere responds to fluctuations in the AMOC, so that the timescales of AMOC variability would control BJC timescales. Likewise, using a hierarchy of models, the role of the ocean in decadal energy compensation was also stressed by (Farneti & Vallis, 2013). Nevertheless, the compensation mechanisms originate (ocean or atmosphere) has not been investigated. Furthermore, while in the atmosphere zonal variations may be not too critical, the respective roles of the Atlantic and the Indo-Pacific basins OHT still need to be explored. Accordingly, the goal of this paper is to explore BJC systematically in a state-of-the-art climate model focusing on its timescale dependence and the roles of the Atlantic and Indo-Pacific. The structure of the paper is as follows: in section **2** we will briefly describe the IPSL-CM6A-LR model, and the BJC diagnostics and methods used. In section **3** we describe BJC in the control experiment of this model, and investigate the mechanisms associated with it on decadal and centennial timescales. In the last section we discuss the conclusion of this study, its implications, and possible topics to explore in the future.

2. Data and Methods

2.1 IPSL-CM6A-LR model

We use a 2000-years long control experiment of the IPSL-CM6A-LR model (Boucher et al., 2020), developed at the Institut Pierre-Simon Laplace (IPSL). The atmospheric component is the general circulation model LMDZ6A-LR (Hourdin et al., 2020). It has a horizontal grid of 144 x 142 points and a resolution of 2.5° × 1.3°. This model uses 79 vertical levels and hybrid sigma-pressure coordinates. The ocean component is the Nucleus for European Modelling of the Ocean (NEMO) which has three major subcomponents: the ocean model NEMO-OPA (Madec et al., 2017), the sea ice dynamics and thermodynamics NEMO-LIM3 (Rousset et al., 2015; Vancoppenolle et al., 2009). The grid follows an eORCA1 configuration in which the horizontal grid has 1° resolution, refined to 1/3 degree of latitude in the equatorial zone. Vertically, there are 75 non-uniform levels, with thicknesses of 1 m near the surface, 10 m at 100 m depth, and approximately 200 m in the bottom layers. A comprehensive analysis of the IPSL-CM6A-LR model components, performance, and improvements in the physics compared to previous versions is presented by Boucher et al., (2020). This model is characterized by a distinctive centennial mode of ocean variability in AMOC (Bonnet et al., 2021; Boucher et al., 2020; Jiang et al., 2021). In the model's 2000-year control simulation we use, the centennial AMOC displays two different regimes: an active period (~ first 800 years) and a subsequent quieter period in the rest of the time series (**Fig. 7b** in section **3**). Subsequently, we use the full timeseries to diagnose BJC and the first 800 years to explore the associated dynamics.

A number of other CMIP6 simulations also show a similar centennial variability (Jackson & Vellinga, 2013; Meccia et al., 2023; Waldman et al., 2021), even though we have not found previous references to regime shifts of the centennial mode. Nevertheless, since the IPSL-CM6A-LR has a spin-up lasting several thousands of years and this mode also survives in long perturbation experiments (Ferster et al., 2021), this behavior is not an adjustment to the initial conditions. Moreover, such regime shifts appear to be part of AMOC natural variability and have been observed in other models as well, albeit for decadal and multi-decadal modes of variability (e.g., Muir and Fedorov 2015, 2017). Indeed, one can expect such regime shifts when the dynamics is controlled by a weakly-damped internal mode sustained by noise.

To verify how the model reproduces MHT and its components, we use observations-based data (Trenberth et al., 2019) (

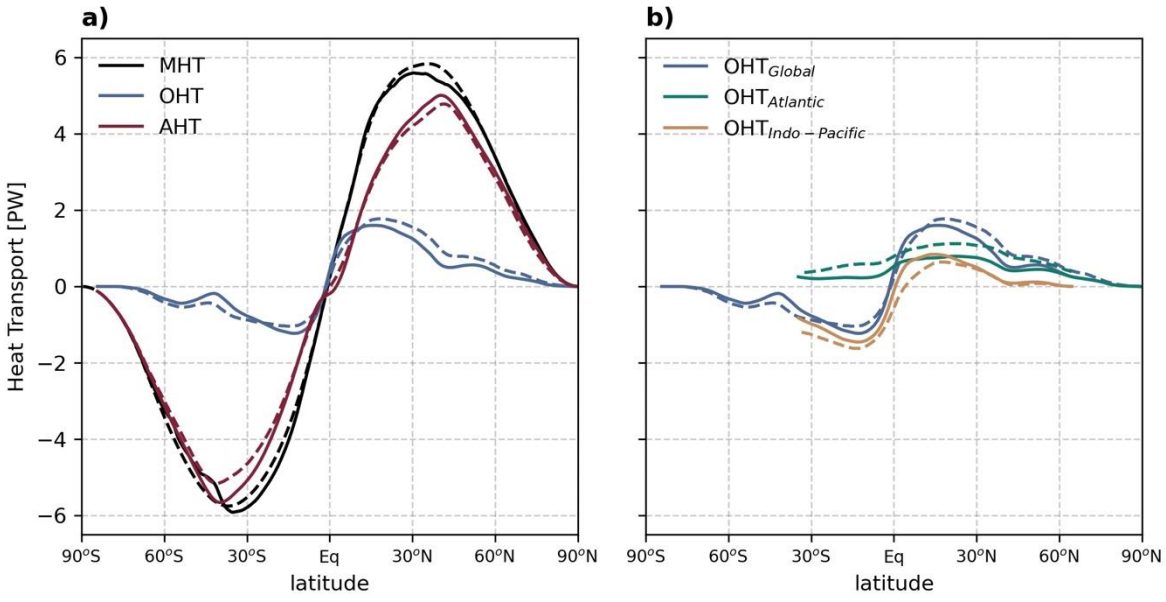

Fig. 1), in which net heat flux at the TOA from CERES-EBAF-TOA (Loeb et al., 2018) was

used to compute the observed MHT and AHT was obtained as a residual. All observations correspond to the [2000-2016] time period. As anticipated, the mean profile of meridional heat transport within the IPSL-CM6A-LR model is characterized by the ocean dominating in the deep tropics while the atmosphere providing by far the largest contribution to MHT poleward of 15°N/S. The Atlantic basin transports heat poleward at all latitudes in the time mean. Overall, the IPSL model is able to represent the meridional heat transport and its components accurately. However, in the northern hemisphere, MHT is slightly underestimated by the model mainly in the tropics and mid-latitudes. The best MHT estimates are at the equator and at high-latitudes. In the Southern Hemisphere, the model overestimates (underestimates) MHT in the tropics (mid-latitudes). The AHT is slightly overestimated in the tropics and mid-latitudes of both hemispheres. Finally, OHT displays an equatorward shift with respect to the observations resulting in a slight overestimation in the deep tropics and an underestimation everywhere else

(

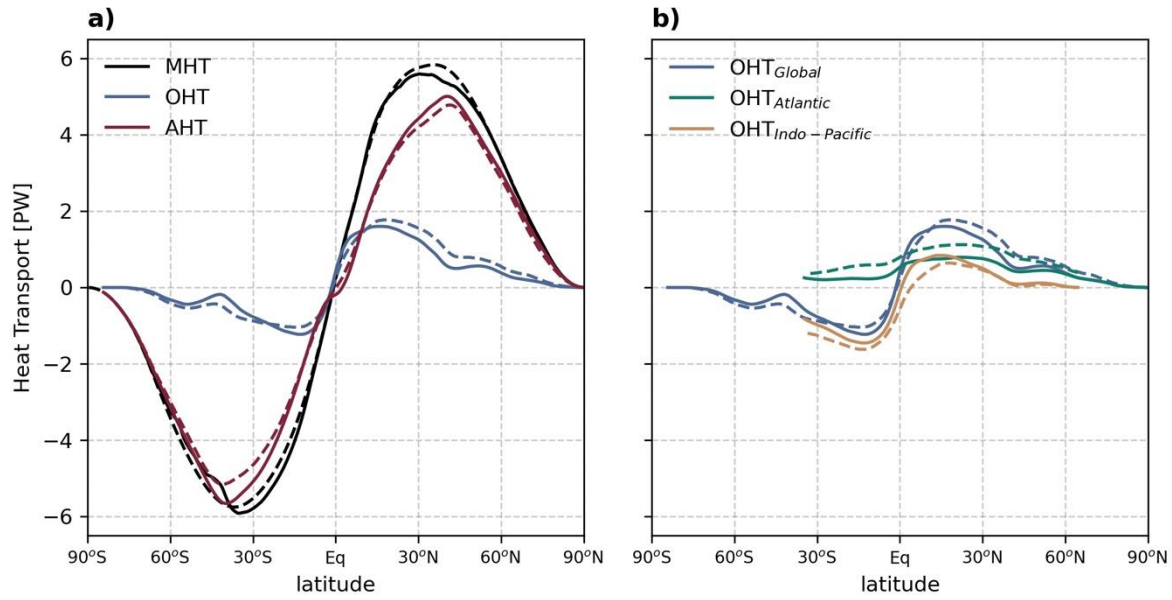

Fig. 1). For the ocean components (

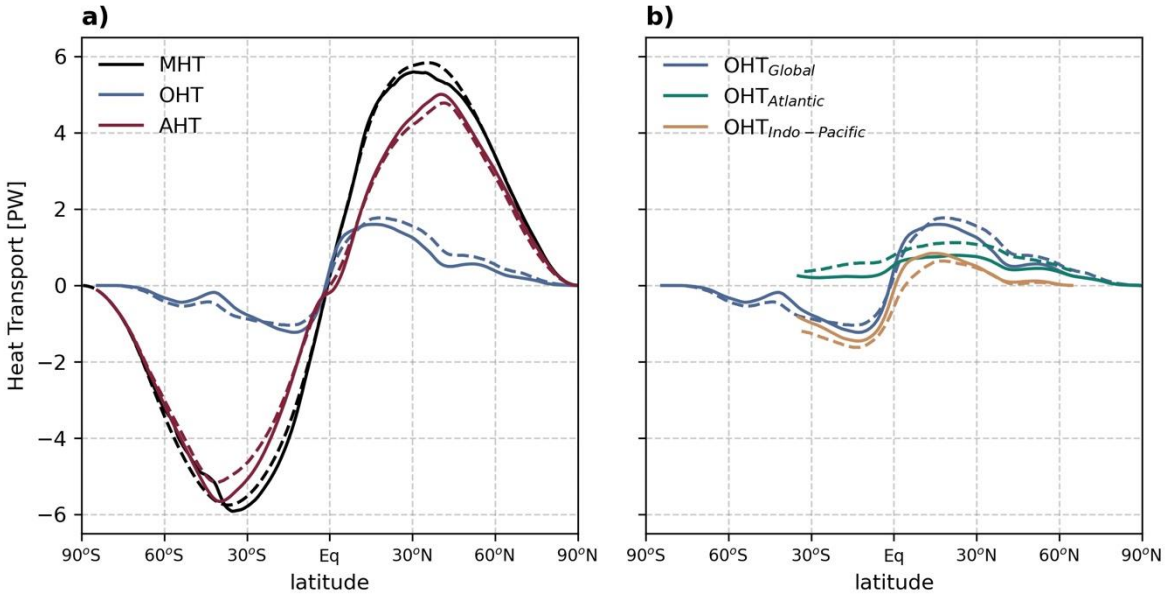

Fig. 1b) we observe that the Atlantic OHT is underestimated at all latitudes while the Indo-Pacific OHT is overestimated south of 30°N.

2.2 Bjerknes compensation diagnostics and mechanisms

Meridional heat transport can be estimated following two approaches (Trenberth & Caron, 2001). The first is an indirect approach where heat transport is approximated by the area-integrated net heat fluxes. This approach is valid assuming that the rate of change of heat content in the fluid layer is negligible. This is a good approximation for the atmosphere but not for the ocean, because of its larger heat capacity. The second method is a direct approach in which the fluid circulation and sub-grid processes are taken into account. We adopt the indirect approach for the atmospheric heat transport following equation (1), where R_e, λ and ϕ are the Earth's radius, longitude, and latitude, respectively. The ocean heat transport is obtained from

the model output, which includes contributions of resolved and parameterized processes (direct approach). The total heat transport is computed integrating the net heat flux at the top of the atmosphere following equation 2. This strategy is well suited for BJC studies as the heat transport components are obtained from independent computations. As the IPSL-CM6A-LR model has a residual drift, albeit relatively small, (Mignot et al., 2021), we remove the drift by computing a linear fit and removing the associated trend before performing any calculation. The area-weighted time-mean is removed from the net heat fluxes at the surface and at the TOA to account for the model energy imbalance at the TOA (of about 0.7 W/m^2).

$$AHT = \int_{-\frac{\pi}{2}}^{\phi}\int_{0}^{2\pi} R_e^2(Q_{toa-}Q_{sfce})\, cos\phi\, d\lambda d\phi \quad (1)$$

$$MHT = \int_{-\frac{\pi}{2}}^{\phi}\int_{0}^{2\pi} R_e^2 Q_{toa}\, cos\phi\, d\lambda d\phi \quad (2)$$

Annual timeseries are smoothed with a Butterworth bandpass filter with frequencies bands of [1/20 -1/80] and [1/80-1/250] 1/year for decadal and centennial timescales, respectively. These two bands capture the peaks of variance of AMOC in the power spectrum, allowing us to contrast the role of the ocean heat content at different timescales. The filter is applied twice (first forward, then backward) in order to conserve the phase of the signals. We identify BJC when linear correlations between anomalous ocean and atmospheric heat transport are negative and statistically significant. The statistical significance at 95 percent is evaluated using the Student *t*-test. The effective degree of freedom was computed as $EDOF = N\Delta t/2\,T_e$ where N,

t and T_e are the length, time resolution and the *e*-folding decay time of autocorrelation of the timeseries, respectively (Panofsky et al., 1958).

In order to distinguish the role played by each heat transport component in BJC, we compute a Turner Angle (*Tu*) based on ocean and atmospheric heat transport anomalies, which is analogous to the Turner Angle used to understand the relative roles of salinity and temperature in the water column stability (Turner, 1973). The BJC Turner Angle is computed following equation (3) where primes indicate anomalies and the bar indicates a time mean. The computed Turner angle indicates whether BJC is full or partial and whether the atmosphere undercompensates or overcompensates variations in ocean heat transport, as described below.

$$Tu = \overline{\tan^{-1}\frac{AHT' + OHT'}{AHT' - OHT'}} \qquad (3)$$

with,

$Tu = 0$ full BJC

$-\pi/4 \leq Tu < \pi/4$ partial BJC

$-\pi/4 \leq Tu < 0$ the atmosphere undercompensates the ocean

$0 \leq Tu < \pi/4$ the atmosphere overcompensates the ocean

To explore the mechanisms associated with BJC at decadal and centennial timescales, we compute an AMOC index as the maximum of the overturning streamfunction in the North Atlantic [20°N-60°N]. To understand changes in the ocean and the atmospheric response

linked to AMOC fluctuations, we perform linear regressions of ocean and atmospheric fields onto the AMOC index. AMOC changes impose hemispherical antisymmetries on temperature and heat transports, while the Intertropical Convergence Zone (ITCZ) tends to shift toward the warmer hemisphere. We explore the correlation of AMOC changes and ITCZ shifts in a BJC context. We use as a proxy of ITCZ location the precipitation centroid, computed as the latitude that splits in two equal parts the tropical precipitation [20°S-20°N]. Then we check if the precipitation centroid is sensitive to changes in AMOC. Since this relationship is strongest in the tropical Atlantic, we only show results for the precipitation centroid over that region.

$$\frac{dOHC}{dt} = -OHT_{\lambda} - OHT_{\phi} + \int Q_{sfce} dA \quad (4)$$

In order to analyse the relative role of the Atlantic and Indo-Pacific OHTs in BJC, we compute the heat budget of the Southern Ocean (SO) and its Atlantic and Indo-Pacific sectors as in equation (4). The rate of change of ocean heat content in that region $dOHC/dt$ is mainly due to contributions from zonal OHT_{λ} and meridional OHT_{ϕ} ocean heat transports and surface heat fluxes integrated over the area of interest, $Q_{sfce} dA$. We note that the model surface heat flux output includes the effect of sea ice. Other terms contributions are considered negligible. When computing the heat budget of the full SO, the term OHT_{λ} vanishes. If we consider 35°S as the boundary dividing the SO from the Atlantic and the Indo-Pacific basins, then the net ocean meridional heat transport into the SO equals the OHT out of the Atlantic at 35°S minus the OHT entering the Indo-Pacific at the same latitude. The difference between $dOHC/dt$ and

$Q_{sfce}dA$, gives the total ocean heat transport convergence, which is the only term that could describe the potential role of the atmosphere in an interbasin exchange. Then, we compare the order of magnitude of total heat transport convergence to the ocean heat transport magnitude.

3. Results

3.1 Decadal BJC

At decadal timescales, BJC occurs in the Southern Hemisphere mid-latitudes (45°S - 65°S) and north of 15°N in the Northern Hemisphere (**Fig. 2a**). No statistically significant decadal Bjerknes compensation is found over the northern deep tropics, the equatorial and southern tropical regions and close to Antarctica. While in the Southern Hemisphere a statistically significant BJC is found strictly over the mid-latitudes, in the Northern Hemisphere BJC is stronger and extends north of 15°N.

We find two local maxima of negative correlation of 0.78 and 0.75 around 38°N and 67°N respectively. These latitudes correspond to the storm track region and the marginal ice zone (MIZ). The strong compensation at these two key latitudes is further described in **Fig. 3**. In these regions large air-sea fluxes and sharp meridional sea surface temperature gradients allow a quick adjustment of the atmospheric circulation. The preferred location of the absolute maximum in the decadal BJC can be model dependent (Outten et al., 2018), but in our model BJC over the storm track region is slightly stronger. The decadal OHT variance is greatest between 40°S and 40°N, while both the OHT and AHT variances are maximum over the storm

track region (**Fig. 3b**). In contrast, their ratio $std(AHT)/std(OHT)$ is larger in the MIZ (**Fig. 3c**).

The time-mean Turner Angle between decadal ocean and atmosphere heat transport anomalies (**Fig. 3d**) reveals that the atmosphere undercompensates the ocean at almost every latitude, except in the MIZ where the ocean and the atmosphere components contribute equally to the BJC (the Turner Angle is close to 0°). Therefore, the latter metric gives results over these regions analogous to the ratio $std(AHT)/std(OHT)$.

Next, we investigate the role of AMOC in decadal BJC. We compute an AMOC index as the maximum overturning volume streamfunction in the North Atlantic [20°N-60°N]. The resulting time series leads OHT over the storm track region by 2 years with a correlation coefficient of 0.62 (by 4 years over the MIZ with a correlation of 0.54). We further investigate changes in the Atlantic circulation at decadal timescales by regressing the overturning volume streamfunction onto the AMOC index (**Fig. 4a**). We observe pronounced changes between 40°N-50°N in the strength and vertical extension of the deep overturning cell. We also analyse the dynamical components of OHT in the Atlantic: OHT due to gyre circulation (OHT-*gyre*), OHT due to meridional overturning circulation (OHT-*overt*) and OHT due to parameterized mesoscale eddy-induced advective transport (OHT-*eddy*) (**Fig. 4c**). We find that changes in the Atlantic OHT are dominated by the overturning circulation south of 45°N while north of this latitude OHT-*gyre* is the dominant component. The OHT-eddy component only changes in a latitude band between 35°N-50°N while representing less than 20% of the total Atlantic OHT

response. We note however that in our model, as in most climate GCMs, the eddy contribution is parameterized and its values can be smaller than the observations.

To understand heat redistribution in the ocean as well as atmospheric response to AMOC and OHT fluctuations, we regress the zonally-integrated Atlantic and Indo-Pacific Ocean heat content and the zonally averaged atmospheric temperature onto the AMOC index (**Error! Reference source not found.**a-c). In the Atlantic, we observe a strong heat gain in the surface layers north of 15°N, and some of Atlantic warm waters penetrating across the MIZ. In the mid-latitudes we find a subsurface cooling associated with the returning flow of North Atlantic deep waters. This heat loss in the mid-latitudes at the subsurface connects with a heat loss region in the tropics near the surface. In the Indo-Pacific as anticipated, the ocean response to AMOC fluctuations is shallow and less pronounced however there is a slight heat gain in the Pacific north of 15°N and heat loss in the tropics. No significant changes are identified below 2500 m. Because AMOC is stronger and there is an anomalous northward OHT in the Atlantic, the atmosphere responds with a pronounced warming in the Northern Hemisphere. This warming is strongest north of 30°N up to 800 mb. As a consequence of the strong atmospheric inter-hemispheric contrast there is a southward compensating AHT.

3.2 Centennial BJC

We now diagnose the centennial BJC, analyse its mechanisms and compare it to the decadal BJC. At the centennial timescales, in contrast to decadal, we find a strong BJC at all latitudes north of 60°S (**Fig. 2a**). The ratio of centennial AHT to OHT is maximum in the tropics (**Fig.**

2b). The standard deviations of centennial OHT and AHT as functions of latitude have similar values, and they are both smaller than decadal values, south of 15°N. North of this latitude, centennial OHT standard deviation is larger than that of the atmosphere and comparable to decadal AHT and OHT variability as a consequence of the AMOC two spectral peaks in the IPSL-CM6A-LR model. The ratio of centennial AHT to OHT (**Fig. 2c**) is largest between 15°S and 15°N, while the Turner Angle (**Fig. 2d**) is smallest, indicating that centennial ocean and atmosphere heat transport anomalies are comparable in this region, contributing to a strong BJC. In the extra-tropics of both hemispheres the atmosphere undercompensates the ocean, except south of 60°S.

The structure of the overturning circulation (**Fig. 4b**) shows that changes in the centennial AMOC spans further South of the Equator when compared to the decadal timescale. The maximum of the anomalous overturning cell lies between 30°N and 45°N, and extends deeper than the model climatology. The Atlantic OHT response to AMOC (**Fig. 4d**) reveals that, as for the decadal case, the pattern of OHT components changes at the latitude of the maximum overturning: south of 40°N major changes in OHT are due to the overturning component, while North of 45°N the gyre contribution dominates. Changes in the centennial AMOC result in a 50% stronger OHT response compared to that of decadal.

The regression of zonally-integrated OHC in the Atlantic at centennial timescale (Error! Reference source not found.**b**) has a similar structure compared to that seen for the decadal timescale. We also observe a heat gain at the surface and heat loss in the subsurface layer

associated with the overturning cell change and the returning flow of deep water formed in the high-latitudes North Atlantic. However, at the centennial timescale, the heat loss expands to the South Hemisphere to include the tropical region, which was not the case for decadal. We also note that the heat lost in the first 1000m in the South Atlantic is compensated by a heat gain in the Indo-Pacific at the same depths and latitudes (Error! Reference source not found.**c**). The atmospheric response to AMOC is similar to decadal but also stronger (Error! Reference source not found.**a**): one part of the heat gained at the ocean surface is released to the atmosphere, then the meridional gradient of temperature decreases inducing an anomalous compensating southward atmospheric heat transport.

Given the dynamical links between AMOC and ocean heat transport and the Hadley Cell and atmospheric heat transport, we explore the covariability of the AMOC and ITCZ at centennial timescales in the context of BJC. Previous studies stressed the role of ocean-atmosphere energy compensation across the equator in connecting ITCZ shifts to AMOC variations (Donohoe et al., 2013; Frierson et al., 2013; Marshall et al., 2014). As a measure of ITCZ location we use the centroid of area-weighted tropical precipitation in the North Atlantic (Donohoe et al., 2013; Frierson & Hwang, 2012). In agreement with the previous studies, we find that ITCZ shifts on centennial timescales correlate well with AMOC changes: the ITCZ shifts northward (southward) when the AMOC becomes stronger (weaker) (**Fig. 7**). This can be explained by a simple consideration: when the AMOC strengthens, this increases oceanic northward heat transport, warming the Northern hemisphere and strengthening the Hadley cell that is located to the south of the ITCZ. The stronger Hadley cell transports more energy across the equator

southward (largely as geopotential energy in the upper troposphere) but more moisture northward (in the lower troposphere), thus shifting the ITCZ northward. This argument implies a full or partial atmospheric compensation of oceanic heat transport variations. Although the precipitation centroid index relates to both ITCZ intensity and location, our results further imply that the ITCZ shift in response to AMOC variations is a consequence of BJC.

To further investigate the potential interbasin compensation between Atlantic and the Indo-Pacific centennial ocean heat transports anomalies (**Fig. 8**) we compute the correlation as a function of latitude between Atlantic and Indo-Pacific OHTs (**Fig. 8a**). We note a strong compensation south of 15°N with correlation values around 0.9. A time-mean Turner Angle between Atlantic and Indo-Pacific OHTs anomalies (**Fig. 8b**) shows that the interbasin compensation originates from the Atlantic. Time series of OHTs at 35°S at each basin (**Fig. 8c**) shows that most of the heat lost by the Atlantic is gained by the Indo-Pacific at the same latitude. We also find a strong interbasin compensation around 45°N. We did not explore it further but we argue that an atmospheric bridge from the North Atlantic to the North Pacific (northward shift of westerlies) may be the cause of the compensation at these latitudes. Since the Pacific lacks a deep reaching overturning cell, the wind-driven ocean gyres are the main mechanism to modulate OHT over that region. Previous analysis suggests that atmospheric westerlies can shift in response to AMOC variations (W. Liu et al., 2020), thus causing changes in the ocean gyre circulation.

The Atlantic and the Indo-Pacific are connected through the SO, which is a large reservoir of heat, where air-sea heat fluxes of large magnitude take place and in which the wind-driven Antarctic Circumpolar Circulation is a major feature. Accordingly, we test the hypothesis that the centennial interbasin exchange occurs effectively through this 'ocean bridge' rather than through an 'atmospheric bridge' by computing the heat budget of the SO (**Fig. 9**). The difference between the rate of change of ocean heat content and the surface heat flux result in the total ocean heat transport convergence, which is the only term that could designate the potential role of the atmosphere in the interbasin exchange. If we consider 35°S as the boundary dividing the SO from the Atlantic and the Indo-Pacific basins, then the net ocean meridional heat transport into the SO equals the meridional heat transport out of the Atlantic at 35°S minus meridional heat transport entering the Indo-Pacific at the same latitude.

Next, we compare the magnitude of total heat transport convergence to the ocean heat transport magnitude. In the Atlantic sector of the SO (**Fig. 9a**) the standard deviation of both meridional and zonal heat transport is around 0.02 PW compared to 0.006 PW for the heat transport divergence. In the Indo-Pacific sector (**Fig. 9b**) the standard deviation of ocean heat transport is 0.01 PW compared to 0.005 PW for the heat transport convergence. In the whole SO (**Fig. 9c**), the meridional heat transport equals the heat transport convergence. All this shows that the centennial interbasin exchange takes place mainly through the ocean and that the atmospheric contribution is one order of magnitude smaller than the ocean terms. During the strong AMOC regime (years 1-800), the Atlantic OHT at 35°S leads by 5 years the Indo-Pacific OHT at the same latitude which is consistent with the former driving the latter. **Fig. 10a-b** summarizes the

interbasin exchange through the ocean bridge: the centennial AMOC anomalies lead the Atlantic OHT at 35°S by 18 years, then the zonal OHT through 20°E by 7 years. This signal propagates into the Indo-Pacific basin 2 years later. The OHT out of the Atlantic at 35°S leads the OHT into the Indo-Pacific by about 6 years.

4. Conclusions and Discussions

In this study a long control run of the IPSL-CM6A-LR model is used to investigate the BJC validity for the model-simulated natural climate variability. Specifically, we investigate BJC on decadal and centennial timescales and the key mechanisms involved. We have proposed a new diagnostic for BJC based on the Turner Angle, which allows us to quantify the relative contribution of ocean and atmospheric heat transport anomalies and thus to distinguish whether the atmosphere undercompensates or overcompensates changes oceanic heat transport.

The decadal BJC is mostly restricted to mid-latitudes in both hemispheres even though it is stronger in the Northern Hemisphere. No BJC is found near the Equator, in tropical regions and close to Antarctica at this timescale. The maxima of the decadal BJC, as found in other models as well, are located in the storm track region and in the marginal ice zone (MIZ). The decadal Turner Angle shows that the atmosphere undercompensates oceanic changes, which confirms in an independent way the central role of AMOC as a source of ocean heat transport (OHT) variations that initiate BJC. The fact that the ocean has a dominant influence on the

atmosphere in the extratropics corroborates the validity of using the Turner Angle to diagnose BJC.

At centennial timescales, the integral of the net heat flux through the TOA and the rate of change of ocean heat content are both an order of magnitude smaller compared to meridional heat transports. In contrast to the decadal case, heat available in the climate system can therefore only be distributed between the ocean and the atmosphere, explaining a stronger BJC at this timescale (anticorrelation larger than 0.8 north of 65°S). Similar to the dynamics on decadal timescales, on centennial timescales the atmosphere undercompensates the ocean. It is interesting that in the tropical regions the magnitude of atmospheric heat transport variations becomes nearly equal to that for oceanic heat transport variations (Fig. 2b). In contrast to the decadal case, centennial AMOC anomalies extend south of the Equator and so does the centennial BJC. The mechanisms driving BJC are similar on decadal and centennial timescales: a strong AMOC produces anomalous northward OHT that warms the high-latitude atmosphere, reducing the meridional temperature gradient and inducing an anomalous southward AHT in compensation (Yang et al., 2017).

Further, we highlight a strong linkage between the centennial AMOC strength and ITCZ meridional shifts as a manifestation of equatorial BJC. This covariability between the AMOC and ITCZ is weaker at decadal timescales, consistent with the lack of decadal BJC near the Equator. This suggests that a strong equatorial BJC is accompanied by ITCZ response to the interhemispheric thermal contrast led by AMOC changes. The ITCZ is sensitive to AMOC

fluctuations only in the tropical Atlantic as the centennial BJC at the Equator is mostly achieved in this basin.

At centennial timescales, we also observe a strong interbasin ocean heat transport exchange between the Atlantic and the Indo-Pacific, which is again led by AMOC changes. This exchange operates as a Bjerknes-like interbasin compensation for which the role of atmosphere is small compared to that of the ocean, and the Atlantic and the Indo-Pacific basins are connected by the Southern Ocean circulation. This interbasin Bjerknes compensation is consistent with an interbasin seesaw induced by the AMOC in the ocean heat content of each basin as described by Sun et al. (2022).

The present analysis has shown the critical role of the Atlantic basin in BJC and the large-scale energetics of the ocean and the atmosphere. The AMOC is a driver of BJC at both decadal and centennial timescales and its meridional extension determines the strength of BJC as a function of latitude. AMOC variability needs to be strong enough (standard deviation larger than 1 Sv in the current model) to observe a robust response in the ITCZ meridional shift, which is itself a part of the atmosphere response responsible for the BJC, as well as to sustain an interbasin BJC-like compensation with the Indo-Pacific in the Southern Hemisphere.

Some of these results are especially pronounced in the part of the IPSL-CM6A-LR control simulation that displays strong centennial AMOC variations. The lack of such clear BJC in the quiescent AMOC phase would need to be further investigated in models that have less active

centennial AMOC variations. The existence of different regimes could also be investigated in other climates (past or scenarios) as such differences can strongly influence the potential role of BJC in climate change.

Acknowledgments. This work has been funded by the Make our Planet Great Again (MOPGA) program and the Agence Nationale de la Recherche ANR under grant agreement ANR-18-MPGA-0001. AVF has also been supported by NSF (AGS-2053096). All data has been retrieved from the Earth System Grid Federation (ESFG) web page (Boucher et al., 2018). The authors acknowledge the suggestions and advice of Francis Codron, Guillaume Gastineau, Weimin Jiang and Juliette Mignot. We also thank John Fasullo and Kevin Trenberth for kindly sharing the data of the reference meridional heat transport of (Trenberth et al., 2019).

5. Declarations

Funding

This work has been funded by the Make our Planet Great Again (MOPGA) program and the Agence Nationale de la Recherche ANR under grant agreement ANR-18-MPGA-0001; additional funding is provided by NSF (AGS-2053096).

Competing Interests

The authors declare no interests to disclose

Ethical Approval

Not applicable

Authors' Contributions

All authors have substantially contributed to this work: YPP wrote the manuscript and performed the computations for analyses. EG, AF and BF contributed to the analysis and writing of the manuscript.

Data Availability

The IPSL-CM6A-LR piControl data was retrieved from the Earth System Grid Federation (ESFG) web page (Boucher et al, 2018). Observed ocean heat transport data is available in https://doi.org/10.5065/9v3y-fn61. The CERES_EBAF_Ed4.0 dataset was downloaded from https://ceres-tool.larc.nasa.gov.

6. References

Barnett, T. P., Pierce, D. W., & Schnur, R. (2001). Detection of Anthropogenic Climate Change in the World's Oceans. *Science*, *292*(5515), 270–274. https://doi.org/10.1126/science.1058304

Barry, L., Craig, G. C., & Thuburn, J. (2002). Poleward heat transport by the atmospheric heat engine. *Nature*, *415*(6873), 774–777. https://doi.org/10.1038/415774a

Bjerknes, J. (1964). Atlantic Air-Sea Interaction. *Adv. Geophys*, *10*, 1–82. https://doi.org/10.1016/S0065-2687(08)60005-9

Bonnet, R., Boucher, O., Deshayes, J., Gastineau, G., Hourdin, F., Mignot, J., Servonnat, J., & Swingedouw, D. (2021). Presentation and evaluation of the IPSL-CM6A-LR Ensemble of extended historical simulations. *J. Adv. Model. Earth Syst.*, *13*(9), e2021MS002565. https://doi.org/10.1029/2021MS002565

Boucher, O., Denvil, S., Levavasseur, G., Cozic, A., Caubel, A., Foujols, M.-A., Meurdesoif, Y., Cadule, P., Devilliers, M., Ghattas, J., Lebas, N., Lurton, T., Mellul, L., Musat, I., Mignot, J., & Cheruy, F. (2018). *IPSL IPSL-CM6A-LR model output prepared for CMIP6 CMIP piControl*. Earth System Grid Federation. https://doi.org/10.22033/ESGF/CMIP6.5251

Boucher, O., Servonnat, J., Albright, A. L., Aumont, O., Balkanski, Y., Bastrikov, V., Bekki, S., Bonnet, R., Bony, S., Bopp, L., & others. (2020). Presentation and evaluation of the IPSL-CM6A-LR climate model. *J. Adv. Model. Earth Syst.*, *12*(7). https://doi.org/10.1029/2019MS002010

Dai, H., Yang, H., & Yin, J. (2017). Roles of energy conservation and climate feedback in Bjerknes compensation: A coupled modeling study. *Clim Dyn*, *49*(5), 1513–1529. https://doi.org/10.1007/s00382-016-3386-y

Donohoe, A., Marshall, J., Ferreira, D., & Mcgee, D. (2013). The relationship between ITCZ location and cross-equatorial atmospheric heat transport: From the seasonal cycle to the Last Glacial Maximum. *J Clim*, *26*(11), 3597–3618. https://doi.org/10.1175/JCLI-D-12-00467.1

Farneti, R., & Vallis, G. K. (2013). Meridional energy transport in the coupled atmosphere–ocean system: Compensation and partitioning. *J Clim*, *26*(18), 7151–7166. https://doi.org/10.1175/JCLI-D-12-00133.1

Ferrari, R., & Ferreira, D. (2011). What processes drive the ocean heat transport? *Ocean Model.*, *38*(3–4), 171–186. https://doi.org/10.1016/j.ocemod.2011.02.013

Ferster, B. S., Fedorov, A. V., Mignot, J., & Guilyardi, E. (2021). Sensitivity of the Atlantic meridional overturning circulation and climate to tropical Indian Ocean warming. *Climate Dynamics*, *57*(9), 2433–2451. https://doi.org/10.1007/s00382-021-05813-w

Frierson, D. M., & Hwang, Y.-T. (2012). Extratropical influence on ITCZ shifts in slab ocean simulations of global warming. *J Clim*, *25*(2), 720–733. https://doi.org/10.1175/JCLI-D-11-00116.1

Frierson, D. M., Hwang, Y.-T., Fučkar, N. S., Seager, R., Kang, S. M., Donohoe, A., Maroon, E. A., Liu, X., & Battisti, D. S. (2013). Contribution of ocean overturning circulation to tropical rainfall peak in the Northern Hemisphere. *Nat. Geosci*, *6*(11), 940–944. https://doi.org/10.1038/NGEO1987

He, C., Liu, Z., & Hu, A. (2019). The transient response of atmospheric and oceanic heat transports to anthropogenic warming. *Nat. Clim. Change.*, *9*(3), 222–226. https://doi.org/10.1038/s41558-018-0387-3

Held, I. M. (2001). The partitioning of the poleward energy transport between the tropical ocean and atmosphere. *J. Atmos. Sci.*, *58*(8), 943–948. https://doi.org/10.1175/1520-0469(2001)058<0943:TPOTPE>2.0.CO;2

Hourdin, F., Rio, C., Grandpeix, J.-Y., Madeleine, J.-B., Cheruy, F., Rochetin, N., Jam, A., Musat, I., Idelkadi, A., Fairhead, L., & others. (2020). LMDZ6A: The atmospheric component of the IPSL climate model with improved and better tuned physics. *J. Adv. Model. Earth Syst.*, *12*(7), e2019MS001892. https://doi.org/10.1007/s00382-012-1343-y

Jackson, L., & Vellinga, M. (2013). Multidecadal to Centennial Variability of the AMOC: HadCM3 and a Perturbed Physics Ensemble. *Journal of Climate*, *26*(7), 2390–2407. https://doi.org/10.1175/JCLI-D-11-00601.1

Jiang, W., Gastineau, G., & Codron, F. (2021). Multicentennial variability driven by salinity exchanges between the Atlantic and the Arctic Ocean in a coupled climate model. *J. Adv. Model. Earth Syst.*, *13*(3), e2020MS002366. https://doi.org/10.1029/2020MS002366

Jungclaus, J. H., & Koenigk, T. (2010). Low-frequency variability of the arctic climate: The role of oceanic and atmospheric heat transport variations. *Clim Dyn*, *34*(2), 265–279. https://doi.org/10.1007/s00382-009-0569-9

Klinger, B. A., & Marotzke, J. (2000). Meridional heat transport by the subtropical cell. *J. Phys. Oceanogr.*, *30*(4), 696–705. https://doi.org/10.1175/1520-0485(2000)030<0696:MHTBTS>2.0.CO;2

Liu, W., Fedorov, A. V., Xie, S.-P., & Hu, S. (2020). Climate impacts of a weakened Atlantic Meridional Overturning Circulation in a warming climate. *Science Advances*, *6*(26), eaaz4876. https://doi.org/10.1126/sciadv.aaz4876

Liu, Z., Yang, H., He, C., & Zhao, Y. (2016). A theory for Bjerknes compensation: The role of climate feedback. *J Clim*, *29*(1), 191–208. https://doi.org/10.1175/JCLI-D-15-0227.1

Loeb, N. G., Doelling, D. R., Wang, H., Su, W., Nguyen, C., Corbett, J. G., Liang, L., Mitrescu, C., Rose, F. G., & Kato, S. (2018). Clouds and the Earth's Radiant Energy System (CERES) Energy Balanced and Filled (EBAF) Top-of-Atmosphere (TOA) Edition-4.0 Data Product. *Journal of Climate*, *31*(2), 895–918. https://doi.org/10.1175/JCLI-D-17-0208.1

Lucarini, V., & Ragone, F. (2011). Energetics of climate models: Net energy balance and meridional enthalpy transport. *Rev. Geophys.*, *49*(1). https://doi.org/10.1029/2009RG000323

Madec, G., Bourdallé-Badie, R., Bouttier, P.-A., Bricaud, C., Bruciaferri, D., Calvert, D., Chanut, J., Clementi, E., Coward, A., Delrosso, D., & others. (2017). NEMO ocean engine. *Earth Prints*. https://doi.org/10.5281/zenodo.3248739

Marshall, J., Donohoe, A., Ferreira, D., & McGee, D. (2014). The ocean's role in setting the mean position of the Inter-Tropical Convergence Zone. *Clim Dyn*, *42*(7), 1967–1979. https://doi.org/10.1007/s00382-013-1767-z

Masson-Delmotte, V., Zhai, P., Pirani, A., Connors, S. L., Péan, C., Berger, S., Caud, N., Chen, Y., Goldfarb, L., Gomis, M., & others. (2021). Climate change 2021: The physical science basis. *Contribution of Working Group I to the Sixth Assessment Report of the Intergovernmental Panel on Climate Change*, *2*. https://doi.org/10.1017/9781009157896

Meccia, V. L., Fuentes-Franco, R., Davini, P., Bellomo, K., Fabiano, F., Yang, S., & von Hardenberg, J. (2023). Internal multi-centennial variability of the Atlantic Meridional Overturning Circulation simulated by EC-Earth3. *Climate Dynamics*, *60*(11), 3695–3712. https://doi.org/10.1007/s00382-022-06534-4

Mignot, J., Hourdin, F., Deshayes, J., Boucher, O., Gastineau, G., Musat, I., Vancoppenolle, M., Servonnat, J., Caubel, A., Chéruy, F., & others. (2021). The Tuning Strategy of IPSL-CM6A-LR. *J. Adv. Model. Earth Syst.*, *13*(5). https://doi.org/10.1029/2020MS002340

Muir, L. C., & Fedorov, A. V. (2015). How the AMOC affects ocean temperatures on decadal to centennial timescales: The North Atlantic versus an interhemispheric seesaw. *Climate Dynamics*, *45*(1), 151–160. https://doi.org/10.1007/s00382-014-2443-7

Oldenburg, D., Wills, R. C., Armour, K. C., Thompson, L., & Jackson, L. C. (2021). Mechanisms of low-frequency variability in North Atlantic Ocean heat transport and AMOC. *J Clim*, *34*(12), 4733–4755. https://doi.org/10.1175/JCLI-D-20-0614.1

Outten, S., & Esau, I. (2017). Bjerknes compensation in the Bergen climate model. *Clim Dyn*, *49*(7), 2249–2260. https://doi.org/10.1007/s00382-016-3447-2

Outten, S., Esau, I., & Otterå, O. H. (2018). Bjerknes compensation in the CMIP5 climate models. *J Clim*, *31*(21), 8745–8760. https://doi.org/10.1175/JCLI-D-18-0058.1

Panofsky, H. A., Brier, G. W., & Best, W. H. (1958). *Some Applications of Statistics to Meteorology*.

Rose, B. E. J., & Ferreira, D. (2012). Ocean Heat Transport and Water Vapor Greenhouse in a Warm Equable Climate: A New Look at the Low Gradient Paradox. *Journal of Climate*, *26*(6), 2117–2136. https://doi.org/10.1175/JCLI-D-11-00547.1

Rousset, C., Vancoppenolle, M., Madec, G., Fichefet, T., Flavoni, S., Barthélemy, A., Benshila, R., Chanut, J., Lévy, C., Masson, S., & others. (2015). The Louvain-La-Neuve sea ice model LIM3. 6: Global and regional capabilities. *GMD*, *8*(10), 2991–3005. https://doi.org/10.5194/gmd-8-2991-2015

Shaffrey, L., & Sutton, R. (2006). Bjerknes compensation and the decadal variability of the energy transports in a coupled climate model. *J Clim*, *19*(7), 1167–1181. https://doi.org/10.1175/JCLI3652.1

Sun, S., Thompson, A. F., Xie, S.-P., & Long, S.-M. (2022). Indo-Pacific warming induced by a weakening of the Atlantic Meridional Overturning Circulation. *J Clim*, *35*(2), 815–832. https://doi.org/10.1175/JCLI-D-21-0346.1

Trenberth, K. E., & Caron, J. M. (2001). Estimates of meridional atmosphere and ocean heat transports. *J Clim*, *14*(16), 3433–3443. https://doi.org/10.1175/1520-0442(2001)014<3433:EOMAAO>2.0.CO;2

Trenberth, K. E., Zhang, Y., Fasullo, J. T., & Cheng, L. (2019). Observation-Based Estimates of Global and Basin Ocean Meridional Heat Transport Time Series. *J Clim*, *32*(14), 4567–4583. https://doi.org/10.1175/JCLI-D-18-0872.1

Turner, J. S. (1973). *Buoyancy Effects in Fluids*. Cambridge University Press. https://doi.org/10.1017/CBO9780511608827

van der Linden, E. C., Le Bars, D., Bintanja, R., & Hazeleger, W. (2019). Oceanic heat transport into the Arctic under high and low CO2 forcing. *Clim Dyn*, *53*(7), 4763–4780. https://doi.org/10.1007/s00382-019-04824-y

Van der Swaluw, E., Drijfhout, S., & Hazeleger, W. (2007). Bjerknes compensation at high northern latitudes: The ocean forcing the atmosphere. *J Clim*, *20*(24), 6023–6032. https://doi.org/10.1175/2007JCLI1562.1

Vancoppenolle, M., Fichefet, T., Goosse, H., Bouillon, S., Madec, G., & Maqueda, M. A. M. (2009). Simulating the mass balance and salinity of Arctic and Antarctic sea ice. 1. Model description and validation. *Ocean Model.*, *27*(1–2), 33–53. https://doi.org/10.1016/j.ocemod.2008.10.005

Waldman, R., Hirschi, J., Voldoire, A., Cassou, C., & Msadek, R. (2021). Clarifying the Relation between AMOC and Thermal Wind: Application to the Centennial Variability in a Coupled Climate Model. *Journal of Physical Oceanography*, *51*(2), 343–364. https://doi.org/10.1175/JPO-D-19-0284.1

Yang, H., Wang, Y., & Liu, Z. (2013). A modelling study of the Bjerknes compensation in the meridional heat transport in a freshening ocean. *Tellus A*, *65*(1), 18480. https://doi.org/10.3402/tellusa.v65i0.18480

Yang, H., Wen, Q., Yao, J., & Wang, Y. (2017). Bjerknes compensation in meridional heat transport under freshwater forcing and the role of climate feedback. *J Clim*, *30*(14), 5167–5185. https://doi.org/10.1175/JCLI-D-16-0824.1

Yang, H., Zhao, Y., & Liu, Z. (2016). Understanding Bjerknes compensation in atmosphere and ocean heat transports using a coupled box model. *J Clim*, *29*(6), 2145–2160. https://doi.org/10.1175/JCLI-D-15-0281.1

Yang, H., Zhao, Y., Liu, Z., Li, Q., He, F., & Zhang, Q. (2015). Heat transport compensation in atmosphere and ocean over the past 22,000 years. *Sci Rep*, *5*(1), 1–11. https://doi.org/10.1038/srep16661

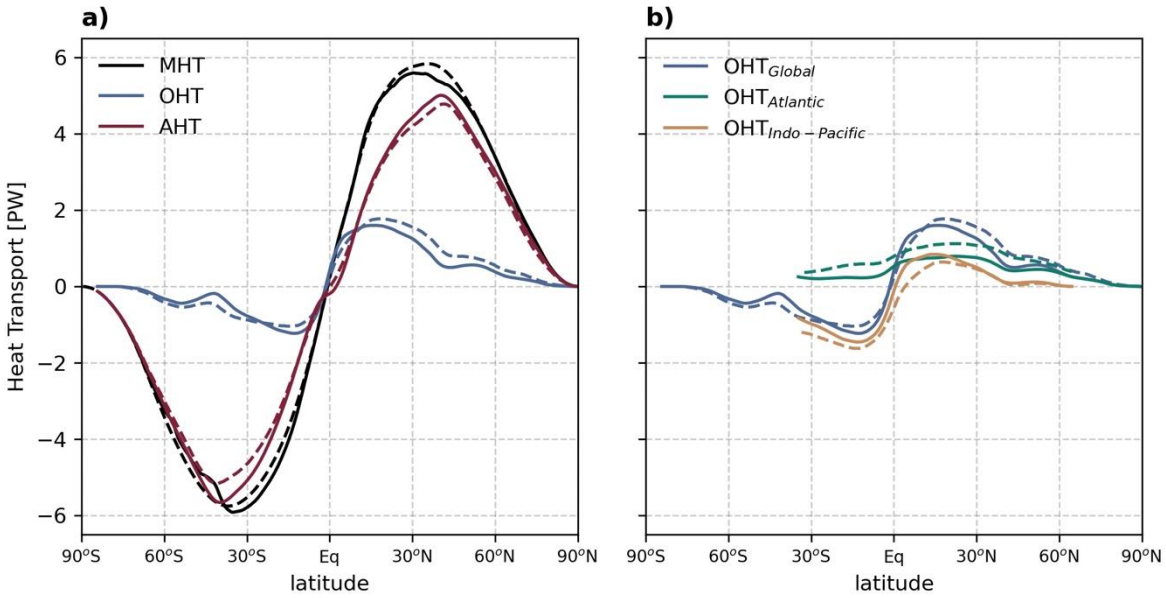

Fig. 1 Time-mean meridional heat transport components in the IPSL-CM6A-LR model. Black, red and blue curves indicate planetary total, atmospheric and oceanic meridional heat transports (MHT, AHT and OHT, respectively). (b) Ocean heat transport and its Atlantic and Indo-Pacific components. Dashed lines show heat transport from observation-based data for the period 2000-2016 (Trenberth et al., 2019).

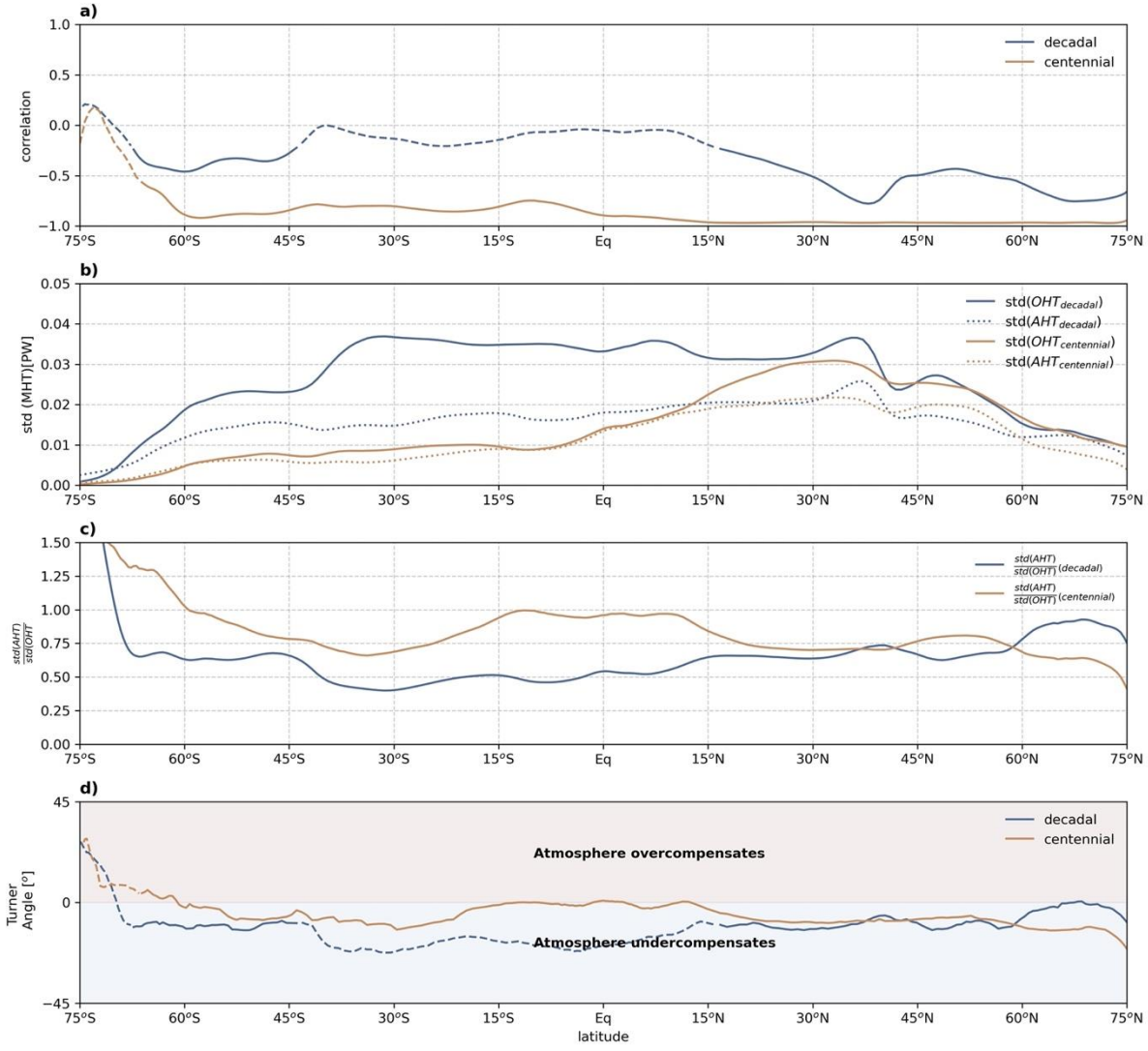

Fig. 2 (a) Correlations between oceanic and atmospheric heat transport anomalies as a function of latitude. The strongest decadal BJC is found around the storm track region (38°N) and the marginal ice zone, MIZ (67°N). To isolate decadal and centennial timescales a Butterworth bandpass-filter is used with time windows of [10-80] and [80-250] years, respectively. (b) Standard deviation of AHT (dotted lines) and OHT (solid lines) as a function of latitude. (c) Ratio of AHT standard deviation to OHT standard deviation. (d) The time-mean Turner Angle (*Tu*) between oceanic and atmospheric heat transport anomalies. Shading indicates that the atmosphere undercompensates (light blue) or overcompensates (light pink) variations in ocean heat transport. Solid curves have correlation values significant at 95 percent according to Student's t-test, while dashed parts of the curves indicate a lower significance. In all panels blue indicates decadal metrics and orange indicates centennial metrics. Computations are based on the entire 2000 years of the control.

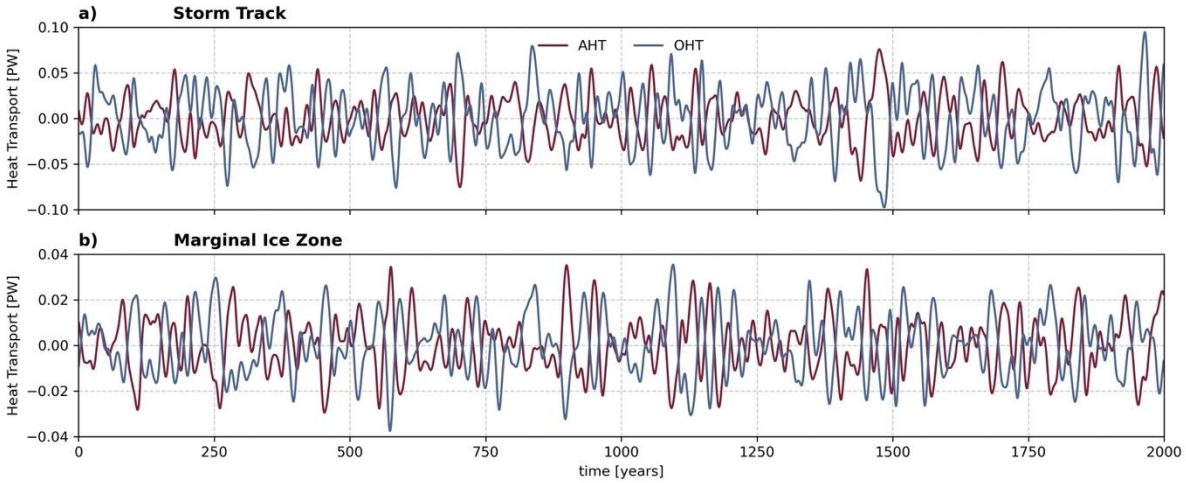

Fig. 3 Time series of ocean and atmosphere heat transport anomalies at the latitudes of the maximum decadal BJC: (a) the storm track region and (b) the marginal ice zone (MIZ). The decadal AMOC index is correlated with OHT at 38°N (67°N) with a coefficient of 0.62 (0.54). A multi-decadal band-pass filter has been applied to the time series (Data and Methods).

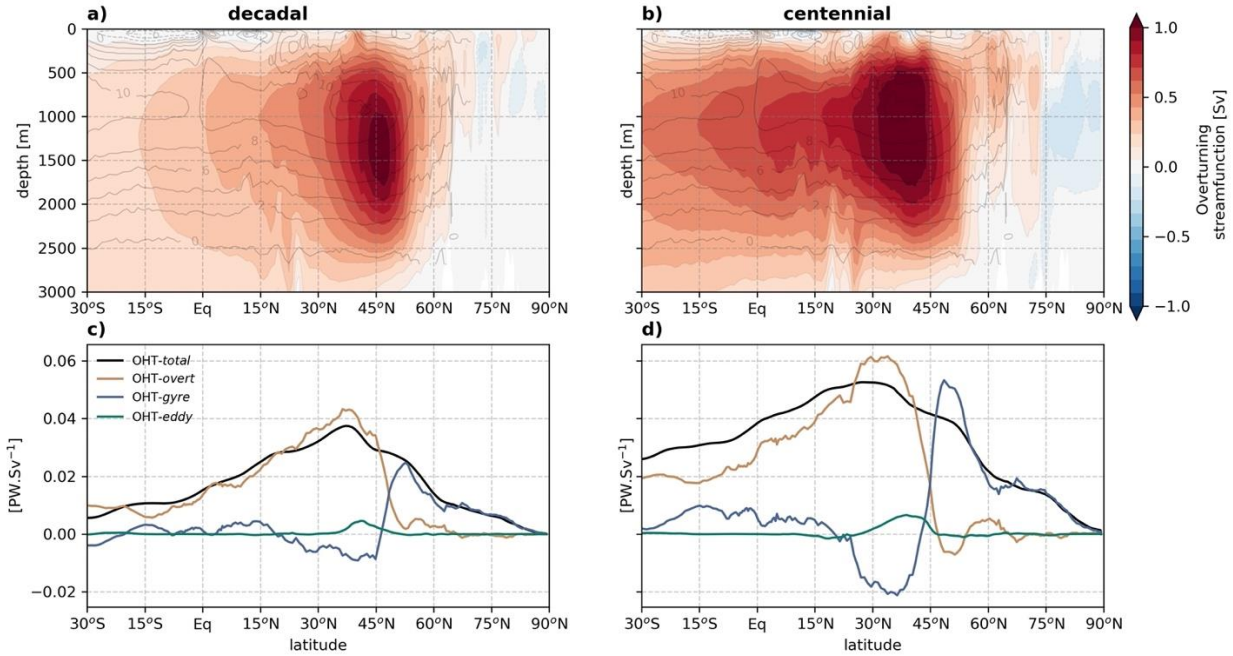

Fig. 4 (a)-(b) Regression of Atlantic overturning volume streamfunction onto the AMOC index for years 1-800 (shading, non-dimensional, i.e., Sv/Sv). Note that on centennial timescales AMOC anomalies extend much farther into the Southern Hemisphere. Contours indicate the time-mean overturning streamfunction with 2 Sv contour intervals (1 $Sv \equiv 10^6 m^3 s^{-1}$). (c)-(d) Regressions of Atlantic ocean heat transport and its components onto the AMOC index for years 1-800.

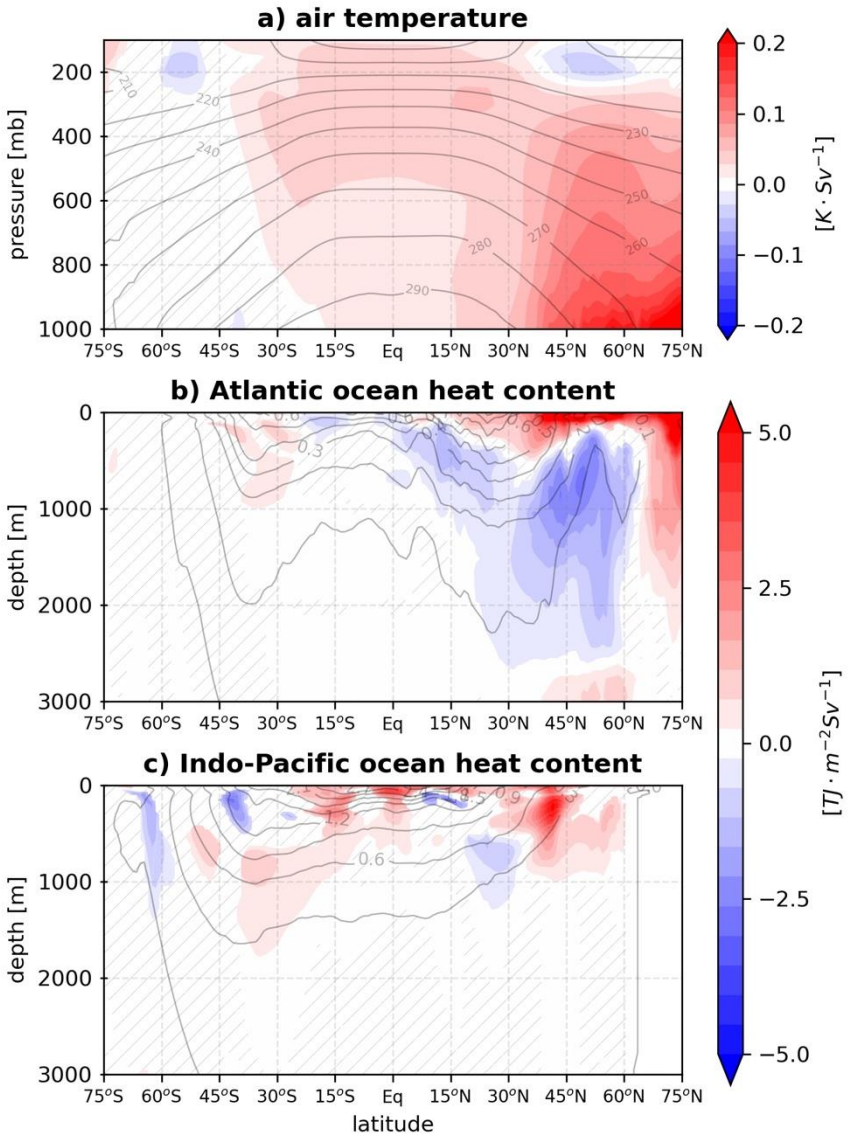

Fig. 5 Regression onto the AMOC index of decadal anomalies of zonally-averaged air temperature (a) and zonally-integrated ocean heat content for the Atlantic (b) and Indo-Pacific (c) for years 1-800 (ocean heat content was integrated from temperature in [°C]). Contours show the time means of the regressed fields (with 10 K contour intervals for the atmosphere, and 0.1 PJ/m^2 for the ocean). Hatched areas indicate significance levels lower than 95 percent according to Student's *t*-test.

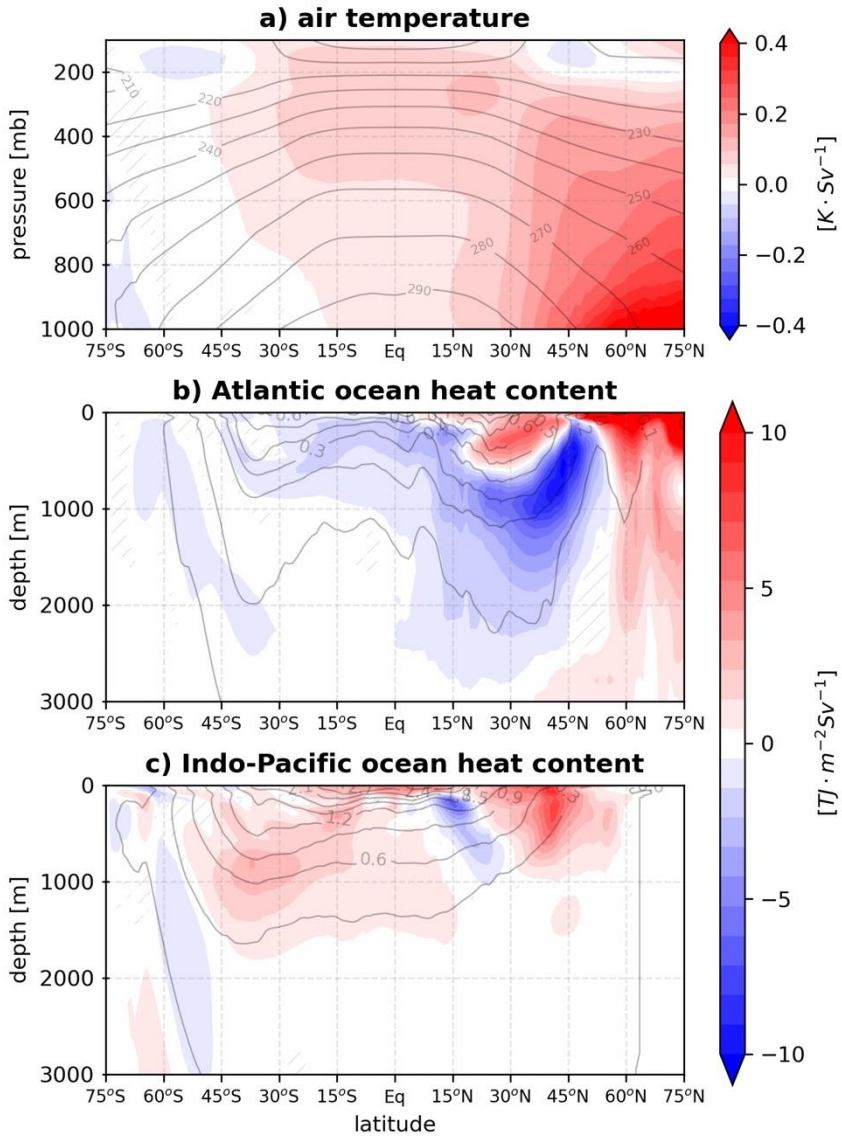

Fig. 6 As in Fig. **5** but for centennial anomalies.

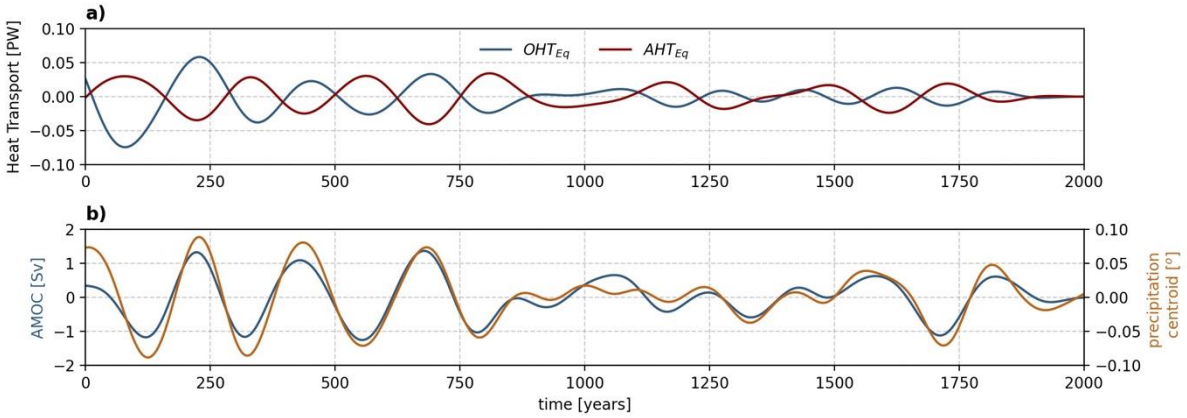

Fig. 7 (a) Centennial cross-equatorial oceanic and atmospheric heat transport anomalies. Annual mean values were computed before applying the centennial band-pass filter. (b) Centennial variations in the AMOC index [Sv] and ITCZ latitudinal position defined as the precipitation centroid [°]. AMOC variations lead ITCZ shifts by about 4 years.

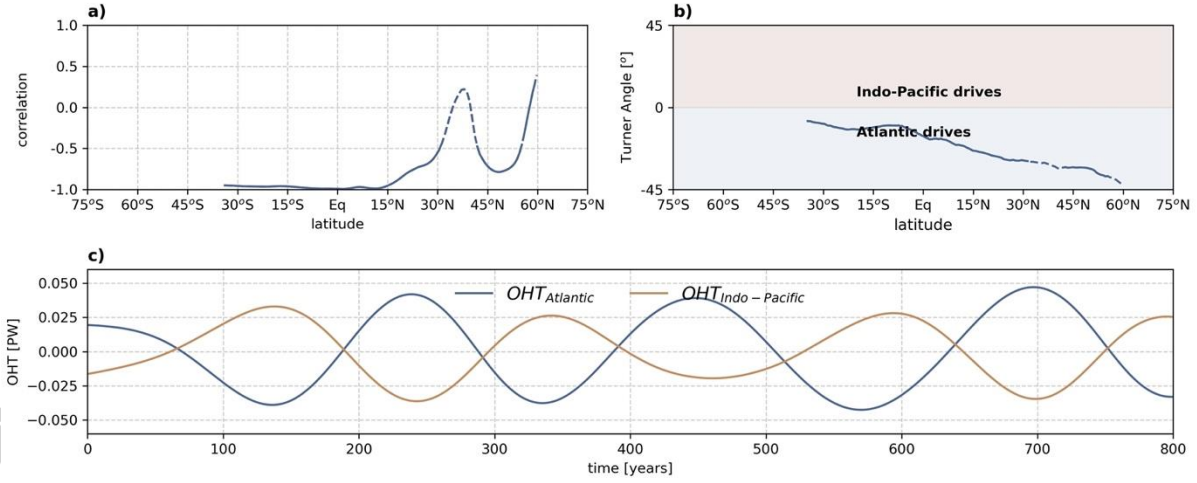

Fig. 8 A Bjerknes-like interbasin compensation (especially pronounced during the strong AMOC variability regime, i.e., years 1-800). (a) Correlation between Atlantic and Indo-Pacific heat transport anomalies as a function of latitude. (b) The Turner Angle for Atlantic and Indo-Pacific heat transport anomalies. Shading indicates whether Atlantic (light blue) or Indo-Pacific anomalies (pink) dominate. (c) Time series of Atlantic (blue) and Indo-Pacific (orange) heat transport anomalies at 35ºS. Solid curves in panels (a) and (b) indicate values significant at 95 percent according to Student's *t*-test. Dashed parts of the curve indicate a lower significance.

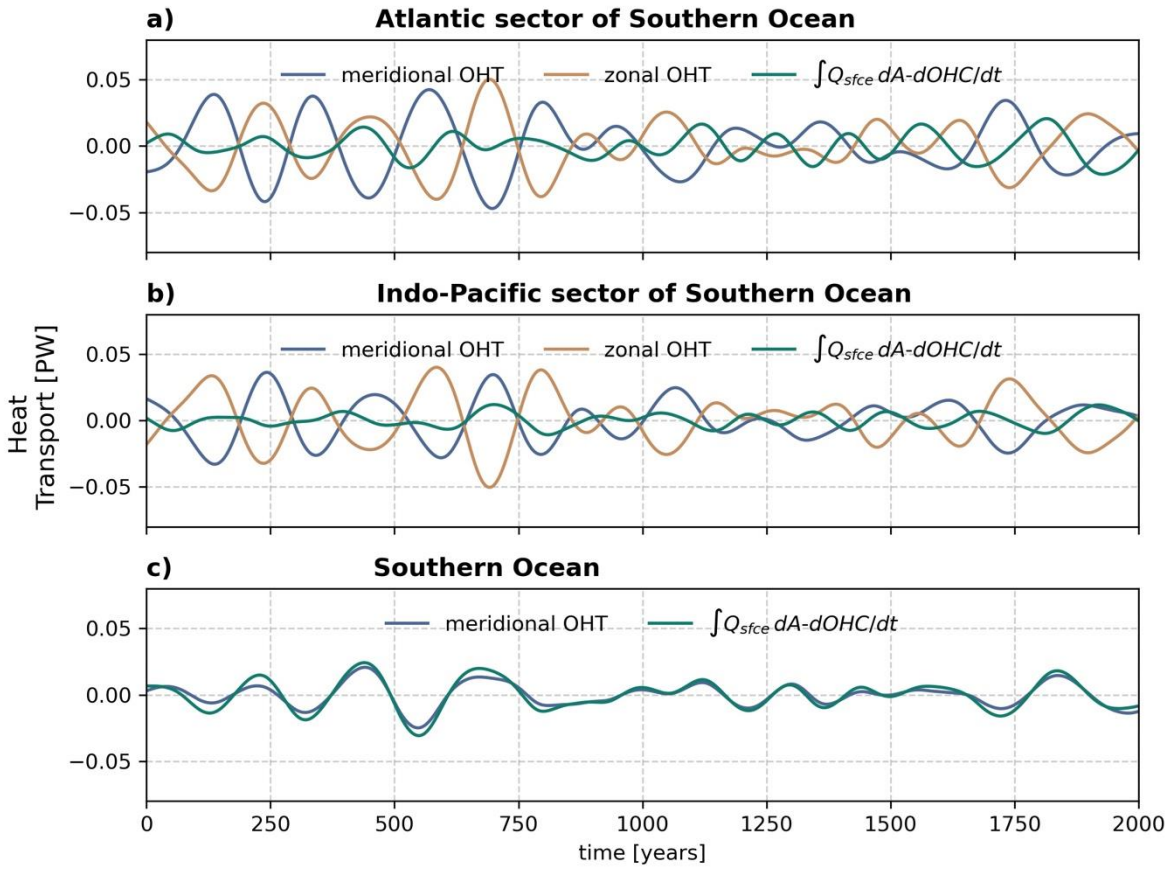

Fig. 9 Heat budget at the centennial timescale for (a) the Atlantic and (b) Indo-Pacific sectors, and (c) the Southern Ocean (for schematics see **Fig. 10**). Blue curves indicate anomalies in the meridional OHT; orange curves indicate anomalies in the zonal OHT; green curves correspond to total OHT convergence for each region. Note that in panels (a) and (b), OHT convergence is significantly smaller than individual OHT terms, which suggests that heat is transported directly between the Atlantic and Indo-Pacific, thus setting the interbasin BJC.

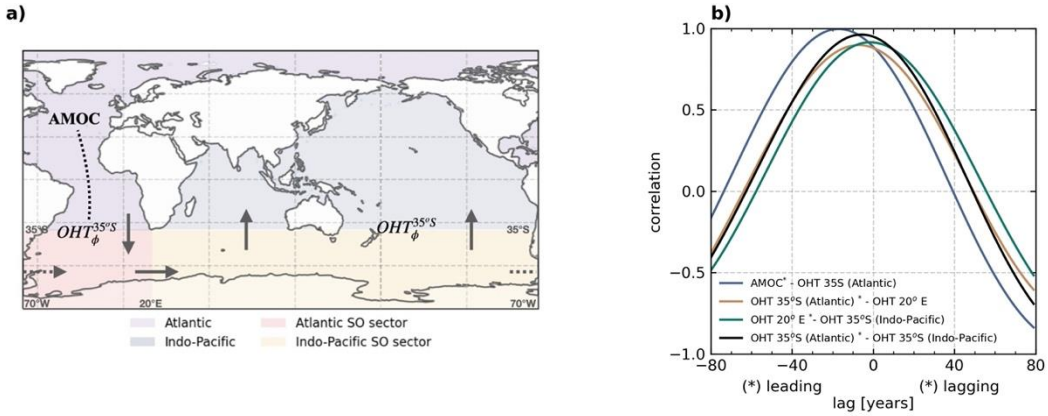

Fig. 10 (a) A schematics for the centennial Bjerknes-like interbasin compensation. Vertical and horizontal arrows represent anomalous meridional and zonal ocean heat transports between the four regions marked in the figure. (b) Lead-lag correlations between the corresponding time series. Negative lags mean that the starred term leads. Solid lines indicate statistical significance at 95 percent according to Student 's t-test.